NANO LETTERS

pubs.acs.org/NanoLett

Letter

DNA Origami Fiducial for Accurate 3D Atomic Force Microscopy Imaging

Pauline J. Kolbeck, Mihir Dass, Irina V. Martynenko,* Relinde J. A. van Dijk-Moes, Kelly J. H. Brouwer, Alfons van Blaaderen, Willem Vanderlinden, Tim Liedl, and Jan Lipfert*

Cite This: *Nano Lett.* 2023, 23, 1236–1243

Read Online

ACCESS | Metrics & More | Article Recommendations | Supporting Information

ABSTRACT: Atomic force microscopy (AFM) is a powerful technique for imaging molecules, macromolecular complexes, and nanoparticles with nanometer resolution. However, AFM images are distorted by the shape of the tip used. These distortions can be corrected if the tip shape can be determined by scanning a sample with features sharper than the tip and higher than the object of interest. Here we present a 3D DNA origami structure as fiducial for tip reconstruction and image correction. Our fiducial is stable under a broad range of conditions and has sharp steps at different heights that enable reliable tip reconstruction from as few as ten fiducials. The DNA origami is readily codeposited with biological and nonbiological samples, achieves higher precision for the tip apex than polycrystalline samples, and dramatically improves the accuracy of the lateral dimensions determined from the images. Our fiducial thus enables accurate and precise AFM imaging for a broad range of applications.

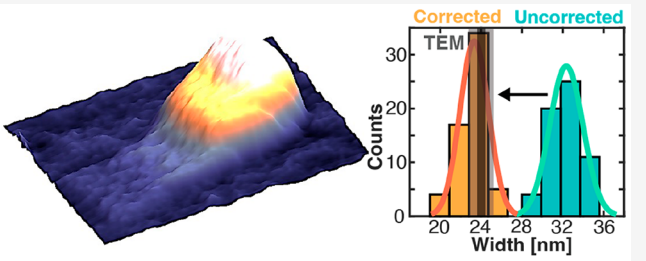

KEYWORDS: *atomic force microscopy, AFM, DNA origami, image correction, tip reconstruction*

Atomic force microscopy (AFM) is a powerful technique to visualize nano- to micrometer-scale structures with subnanometer resolution.[1] Consequently, AFM imaging is frequently used in a broad range of applications, ranging from solid-state physics, to nanofabrication, photonics, material science, and life sciences.[2−8] In particular, AFM imaging has provided unprecedented insights into the structure of biological macromolecules and their complexes.[9−16] For the interpretation and modeling of the imaged structures, high-resolution AFM images that reflect the true sample dimensions are desirable. However, AFM images are distorted due to the finite size of the AFM tip, resulting in a dilation of image features similar to the convolution of optical images by the point-spread function of the imaging system.[5] In general, as long as the tip is much sharper than the feature under observation, the measured profile will closely resemble the true shape. Yet, if the sample contains features whose aspect ratio is comparable to that of the tip, distortions due to the finite size of the tip become significant. To correct for the distortions introduced by the tip one can, in principle, estimate the tip geometry and use it to correct the image and estimate the true specimen shape.[17−20] Unfortunately, the exact shape of most commercial AFM tips is not precisely known. Moreover, the tip shape is variable, even within the same batch of tips, and can also change during the measurement due to wear or contamination of the tip while imaging.

There are several approaches to determining the AFM tip shape. Villarrubia showed mathematically that the best possible estimate of the tip shape is achieved using a method called "blind tip reconstruction".[17] The approach is based on exploiting features of the AFM image as broadened, inverted replicas of the tip. The fidelity and quality of this tip reconstruction depend on the calibration sample containing features with similar or greater sharpness than those of the tip. There are commercially available calibration samples, for example, polycrystalline or silicon standards, with features sharper than the tip[21] or nanofabricated tip characterizers.[22] Inconveniently, these types of calibration samples must be measured either before or after the actual measurement of interest. In addition, since these types of calibration samples are typically very hard, the shape of the tip is prone to change due to wear when the sample is scanned, which will deteriorate or invalidate the resulting tip reconstruction.[18,20] In addition, measuring separate calibration samples cannot correct for changes in tip shape during measurement.

Consequently, it is desirable to use an internal marker, i.e., a reference sample, that is codeposited with the sample of interest. Using an internal reference sample has the advantage that the tip can be characterized during the measurement,

Received: November 2, 2022
Revised: December 25, 2022
Published: February 6, 2023

https://doi.org/10.1021/acs.nanolett.2c04299
Nano Lett. 2023, 23, 1236–1243

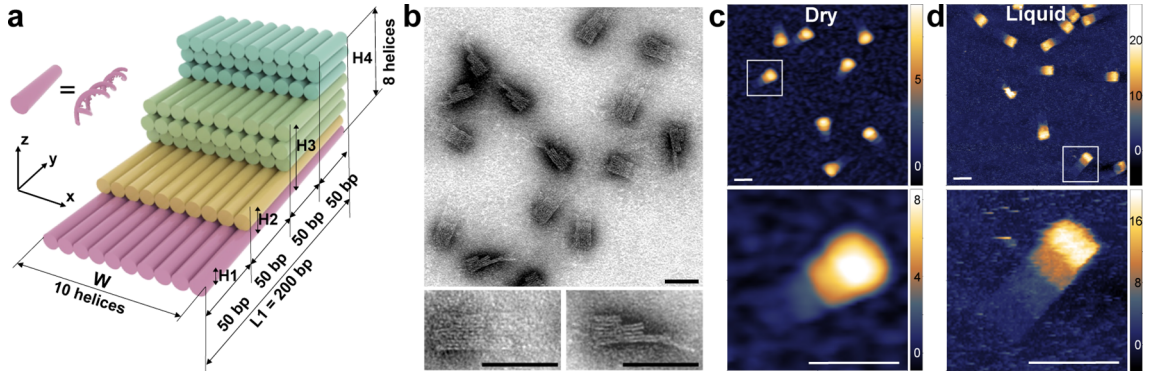

Figure 1. Design of the 3D DNA origami structure used as a fiducial for AFM imaging and visualization by TEM and AFM imaging. (a) Schematic of the designed 3D structure including the design dimensions. The colors represent the different levels. (b) Negative-stain TEM images of the fiducial structures confirm the correct assembly and dimensions (a detailed dimension analysis is shown in Supporting Figure S2). The lower images are zoom-ins of two exemplary structures. (c) AFM height image of the fiducial structures obtained by imaging on APS mica after drying. The upper and lower image both have a resolution of 0.5 pixel/nm. The lower image is a zoom-in of the upper image (white box). (d) AFM height image of the fiducial structures obtained by imaging on APS mica in liquid. Both images have a resolution of 1 pixel/nm. The lower image is a zoom-in of the upper image (white box). The scale bars in all panels are 50 nm. *z*-ranges are indicated in nm by the scale bars on the right.

which is experimentally convenient and ensures that the reference sample and the sample of interest are imaged with identical parameters since, e.g., molecular deformations depend on the AFM imaging mode, the applied force, and the imaging medium. A common internal marker for biological samples is double-stranded DNA[13,23,24] since it is easy to prepare and handle, biocompatible, and well characterized. However, using DNA as a reference sample only works well for samples with a maximum height similar to DNA (1−2 nm depending on the measurement method and force), whereas for higher structures the tip is not sufficiently characterized since the tip reconstruction requires calibration features of the same height as the sample of interest. Another choice for internal, nondestructive markers is virus particles, e.g., the rod-shaped tobacco mosaic virus (TMV),[25] or inorganic nanoparticles.[26,27] However, these are significantly higher than many biologically relevant samples and do not exhibit sharp features, which limits the quality of a blind tip reconstruction.

To overcome these limitations, we present a DNA origami fiducial that provides a 3D reference sample for AFM tip reconstruction with defined, sharp steps of different heights and a height profile well matched for use with a broad range of macromolecular complexes (up to 18 nm). The DNA origami technique enables the self-assembly of large numbers of identical nanostructures at the molecular scale,[28,29] with customized geometry and almost atomistic structural detail.[30,31] The resulting nanostructures have been shown to be robust and stable in a variety of conditions and are used in a large range of applications.[32−39] In particular, DNA origami structures have been used as molecular rulers[40] for fluorescence[41,42] and super-resolution microscopy.[43] For AFM imaging, a single-layer rectangular sheet DNA structure has been used as a size reference and positioning platform.[32,44,45] Yet, the previous structures are not suitable for tip characterization because of their low height and lack of sharply defined features in the *z*-dimension.

Our DNA origami fiducial combines several characteristics that make it well-suited for blind tip reconstruction: the structural features of DNA origami structures have been characterized with high resolution, and their designed structure contains flat faces in the $x-y$ direction and sharp edges in the z direction, creating a four-step staircase from 1 to 2 to 15−20 nm, well matched to typical macromolecular complexes. The fact that it consists of DNA makes it fully biocompatible and enables straightforward surface deposition alongside other biological macromolecules. In addition, we show that our fiducial can be deposited on various surfaces including bare mica, poly-L-lysine (PLL)-coated mica, and aminopropylsilatrane (APS)-coated mica and imaged both dry and in liquid. Taken together, our fiducial enables straightforward AFM image correction for a wide range of nanostructures.

Design of the DNA Origami Fiducial Structure. We designed the staircase-like nanostructure built of eight layers of parallel helices arranged on a square lattice[31,46] (Figure 1a and Supporting Figure S1). The designed length ($L1$) of the structure is 200 base pairs (bp); the maximum height ($H4$) is eight helices; and the width (W) is ten helices. For design purposes, we model DNA helices as a cylinder with a diameter of 2 nm (helix diameter in B-form DNA is 2 nm) and a length of 0.34 nm per bp. Using these parameters and assuming close packing, the approximate size of the designed structure is 68 × 20 × 16 nm^3 ($L1 \times W \times H4$).

We vary the number of DNA helices in the layers to obtain four discrete steps with equal areas and heights of one, two, five, and eight helices. Therefore, the fiducial structure features different heights between 2 and 18 nm, which cover a height range suitable for a broad range of samples, including other DNA origami structures[31,47,48] and biological samples.[11,13,49−51] Critically, the structure provides sharp and defined vertical edges, which is desirable for a reliable AFM tip estimation via blind tip reconstruction.

Confirmation of Correct Folding and Visualization of the Fiducial Structures. We folded the fiducial structures in Tris/EDTA/$MgCl_2$ buffer, purified excess DNA staple strands, and imaged them with negative-stain transmission electron microscopy (TEM; Figure 1b). The fiducial structures appear as rectangular four-"stair" structures with visible striations running along the length of the fiducial, confirming the direction of the DNA helices. The observed structures lay in different orientations on the surface, while defective or deformed fiducials were not observed, which confirms successful and high-yield assembly of our fiducial structures. Using the TEM images, we analyze the dimensions of the fiducial structures (Supporting Figure S2) and find $L1$ = (71.7

https://doi.org/10.1021/acs.nanolett.2c04299
Nano Lett. 2023, 23, 1236−1243

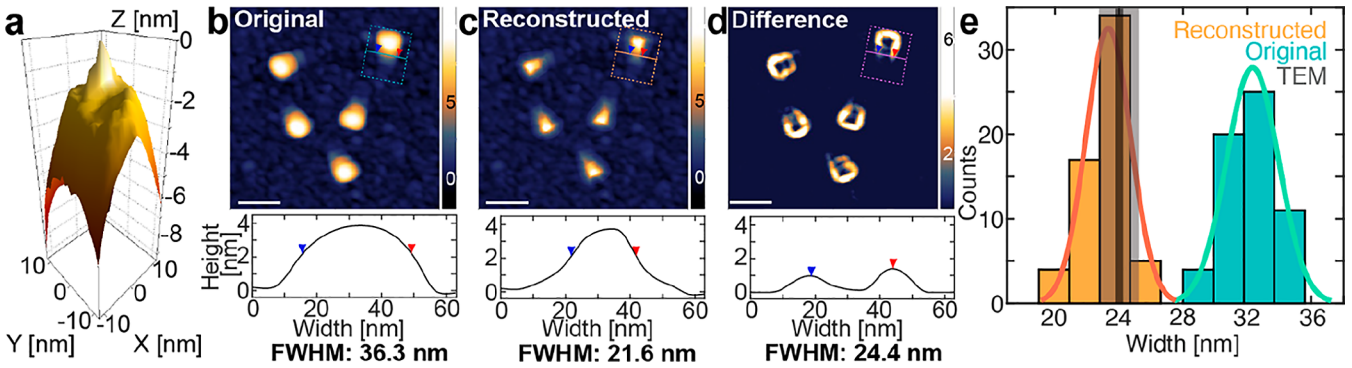

Figure 2. AFM tip characterization and finite tip size correction using the fiducial. (a) Estimate of the AFM tip shape obtained by blind reconstruction using the image shown in Supporting Figure S3c. (b) Top: AFM height image of the fiducial structures on APS mica imaged dry with a resolution of 1 pixel/nm. Bottom: height profile of one exemplary molecule, averaged along the fiducial's long axis (as indicated in the AFM image). Arrows indicate the fwhm;[64] the apparent width is significantly larger than the expected width from the design of ∼22.5 nm and the width measured in negative stain TEM, (23.0 ± 1.2) nm. (c) The same image as in panel b after reconstruction based on the tip shape in panel a from blind tip reconstruction. The apparent width now is much closer to what is expected from the design. (d) Difference image visualizing the effect of image deconvolution. Scale bars are 50 nm, and *z*-ranges are indicated in nm on the right. (e) Width distribution from AFM images before (turquoise) and after (orange) image reconstruction. The solid lines are Gaussian fits. The width of (32.3 ± 1.6) nm (mean ± std) is corrected to (23.3 ± 1.4) nm after correcting for the finite tip size. The corrected value is in excellent agreement with the designed width and the width measured in negative stain TEM indicated by a dark gray vertical line and std in light gray (see Supporting InformationTable S1 for a detailed dimension comparison).

± 3) nm, *H*4 = (19 ± 1.2) nm, and *W* = (23 ± 1.2) nm, indicating an effective diameter of the DNA helices of (2.3 ± 0.1) nm (Supporting Table S1). The effective diameter of DNA helices in 3D DNA origami may vary significantly depending on the DNA origami design, type of packing of the adjacent helices in lattices, number of connecting crossovers, and position of nicks.[52−54] In addition, the spacing of helices depends on solution conditions, like pH, temperature, and in particular ion concentration, as the highly negatively charged helices tend to repel each other electrostatically,[55] resulting in "swelling" of the structures.[53,54] Our value from TEM analysis is in good agreement with the value determined previously under similar conditions for a multilayer origami also by TEM (2.25 nm)[52] and is close to but slightly smaller than the values determined by SAXS in free solution (∼2.7 nm)[53] and cryo-EM structure modeling (∼2.6 nm).[56]

Next, we imaged the fiducial structures by AFM both *in situ* (i.e., fully hydrated under buffered solution) and after drying in air. For dry AFM measurements (Figure 1c), we investigated different surface deposition strategies: bare mica, APS mica, and PLL mica. All surface deposition strategies result in overall similar images, however, with slight differences in the exact dimensions (Supporting Figure S3). Notably, almost all fiducials have the expected shapes and are oriented with their large flat face on the substrate's surface, exposing the staircase feature to the AFM tip, which is also the preferred orientation for our purposes (Supporting Figure S3d). The heights of the steps are almost a factor of 2 lower compared to the heights obtained via TEM (Supporting Figure S4 and Table S1), which is expected for dry AFM measurements.[57] Furthermore, it is apparent from the AFM images that the lateral *x*−*y* dimensions are distorted; in particular, the higher features of the staircase appear wider than the lower features (Figure 1c), which is expected due to the finite size and conical shape of the tip. In AFM images obtained in liquid (Figure 1d), we see different orientations of the fiducial structure on the surface; however, the flat side of the staircase is still attached to the bottom most frequently (Supporting Figure S3d). Compared to the dry measurements, the structures are significantly higher and appear less distorted, resulting in dimensions closer to those measured in the TEM images. Overall, the images obtained in liquid appear "crisper", with higher resolution, which is likely due to the lower interaction forces between the tip and the sample.[19,58]

Fiducial Structures Enable AFM Tip Characterization via Blind Tip Reconstruction and Subsequent Correction for the Finite AFM Tip Size. To test the performance of our DNA origami fiducial structure for estimation of the 3D shape of the AFM tip during measurement, we deposited DNA origami fiducial structures on APS mica and imaged a large field of view (Supporting Figure S3c). We then use the features of the DNA origami fiducials to perform blind tip reconstruction following the protocol of Villarrubia[17] implemented in the image analysis software SPIP or Gwyddion (Figure 2a; see Supporting Information for details, including an example image and step-by-step instructions on how to perform the image reconstruction). We note that the blind tip reconstruction does not require exact knowledge of the reference structure shape, but only requires the fiducial to have sharp and high enough features. In a next step, we use this tip estimate to correct a zoom-in of the same AFM image scanned with the same tip (Figure 2b,c). To assess the effectiveness of this method, we determine the width of the fiducial structure before and after correction and find that the width is reduced from 32.3 to 23.3 nm (Figure 2e), which is much closer to the width of the origami design (Figure 1a) and the width measured in TEM images (Supporting Figure S2). To highlight the finite tip size correction, we also calculate a difference image of the corrected image and the original image (Figure 2d), which shows that especially the widths of the higher steps of the staircase are significantly overestimated in the original image. We note that while the tip size correction procedure does reduce the measured width of the structures imaged in liquid, the final size is still wider than what is observed from corrected AFM images in air or from TEM imaging, but in agreement, within experimental error, with the helix spacing from solution X-ray scattering (∼2.7 nm)[53,54] (Table S1). The difference in observed lateral width per helix,

https://doi.org/10.1021/acs.nanolett.2c04299
Nano Lett. 2023, 23, 1236−1243

(2.33 ± 0.14) nm vs (2.88 ± 0.29) nm/helix after tip shape correction for images in air and in liquid, respectively, is consistent with the view that origami structures swell in solution, due to electrostatic repulsion.[53,54]

Evaluation of the Number of Fiducial Structures Required for Reliable Tip Reconstruction. We next investigate how many fiducial structures are sufficient to get a good estimate of the AFM tip shape. From an image with 114 fiducial structures in total (Figure 3a), we selected between 1 and 100 structures for the blind tip reconstruction. For each number of structures, we randomly selected (with repeats) 20 sets of fiducial structures as inputs for the tip reconstruction. The resulting *x*- and *y*-profiles of the estimated tip shape (Figure 3b,c) converge toward the final tip shape result (100 fiducial structures, dark red line) for ≥10 fiducials (Figure 3d). The results suggest that using a minimum of 10 fiducials for blind tip reconstruction is sufficient for an acceptable tip estimate; for example, for a 1 × 1 μm^2 image this requires a fiducial concentration of ∼1 nM.

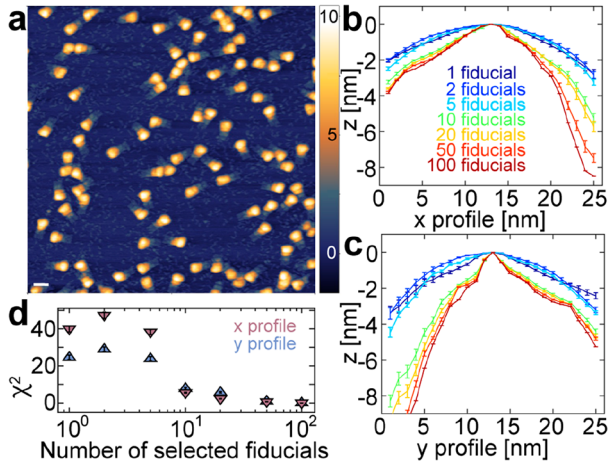

Figure 3. AFM tip characterization using different numbers of fiducials. (a) AFM height image of fiducial structures (114 in total) imaged in dry AFM mode on APS mica with a resolution of 1 pixel/nm. The scale bar is 50 nm, and the *z*-range is indicated in nm on the right. (b) Estimate of the AFM tip shape *x*-profile obtained by using between 1 and 100 fiducials for the blind tip reconstruction in the image shown in panel a. For each graph, 20 sets of fiducials were randomly selected, with repeats. (c) AFM tip shape *y*-profile, analogous to panel b. (d) χ^2 of the *x*- and *y*-profiles shown in panels b and c as a function of the number of selected fiducials compared to the estimate using 100 fiducials with $\chi^2 = \sum_i \frac{(\text{profile}_i - \text{profile}_{100})^2}{\text{profile}_{100}}$. The symbols and error bars are the mean ± std over the 20 sets of randomly chosen fiducials. Error bars are smaller than symbols in some cases.

Comparison of Tip Characterization Using Our Fiducial or a Polycrystalline Sample. Having established an effective method of finite-size tip correction using a DNA origami fiducial structure, we compare our method to correction using an external polycrystalline tip characterization sample (PA01 AFM Tip Evaluation Sample, NanoAndMore GmbH, Germany). We characterized five different AFM cantilevers (FASTSCAN-A, Bruker, USA; which are used throughout the study), using both our fiducial as well as a polycrystalline sample (Supporting Figure S5). Interestingly, we find that for a sharp tip (Supporting Figure S5a−c) we get an extremely good estimate of the very edge of the tip when using the DNA fiducial, almost identical with the vendor specifications and better than the estimate obtained with the polycrystalline sample. The advantage of the polycrystalline sample is that it can characterize a larger *z*-range of the tip (20−30 nm instead of 5−10 nm for the fiducial sample). For a contaminated or blunt tip (Supporting Figure S5d,e), both samples give equally poor results. The results highlight significant tip-to-tip variation even for fresh tips from the same batch. While the polycrystalline sample has the advantage of presenting features with a greater range of heights, for the height that is accessible with our DNA origami fiducial, the DNA fiducial provides a higher-resolution tip reconstruction.

Codeposition of Fiducial Structures Allows Reconstructing the Size of a 24-Helix Bundle DNA Origami Structure. We next test the application of our fiducial *in situ* by codeposition with another structure of interest. We deposited an equimolar mixture of the fiducial sample and a 24-helix bundle DNA origami (24-HB; Figure 4a). In a 1 × 1 μm^2 image (1024 × 1024 pixels), we select 25 fiducial structures for blind tip reconstruction to ensure convergence of the tip estimate (Figure 4b,c). We then use the tip to correct the dimensions of the 24-HBs (Figure 4d−f). The width of the

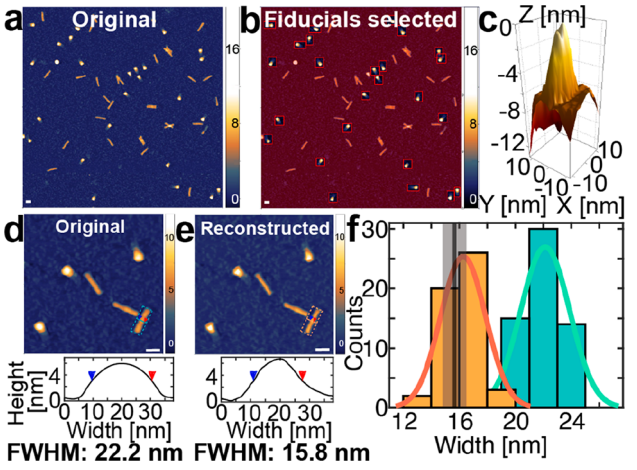

Figure 4. Fiducials enable accurate AFM measurements of a 24-helix bundle DNA origami structure. (a) AFM height image of the fiducial structures codeposited with a DNA origami 24-helix bundle (24-HB) structure, both at a concentration of 1 nM, deposited on APS mica and measured dry with a resolution of 1 pixel/nm. (b) Same image as in panel a, with the 25 fiducial structures highlighted by red boxes. The image sections highlighted by the boxes are used for blind tip shape reconstruction. (c) Tip shape obtained from blind tip reconstruction using the fiducial samples marked in panel b. (d) Top: zoom-in on a different spot of the same sample shown in panel a. The resolution is 2 pixel/nm. Bottom: height profile of the raw AFM image of an exemplary 24-HB. Arrows indicate the fwhm; the apparent width of 22.2 nm is significantly larger than the expected width from the design of ∼15.5 nm. (e) Top: the same image as in panel d, after reconstruction based on the tip shape from blind tip reconstruction shown in panel c. All scale bars are 50 nm, and *z*-ranges are indicated in nm on the right. Bottom: height profile of the reconstructed AFM image of the same 24-HB. (f) Width distribution from AFM images before (turquoise) and after (orange) image reconstruction. The solid lines are Gaussian fits. The width of (22.1 ± 1.8) nm (mean ± std) is corrected to (16.3 ± 1.6) nm by finite tip size correction. This value is in excellent agreement with the designed width of (15.5 ± 1.0) nm, indicated by a dark gray vertical line and std in light gray.

https://doi.org/10.1021/acs.nanolett.2c04299
Nano Lett. 2023, 23, 1236−1243

24-HB is (22.1 ± 1.8) nm (mean ± std; Figure 4f) in the original image, which is significantly larger than the expected width from the design of (15.5 ± 1.0) nm. In contrast, in the corrected image, we find a width of (16.3 ± 1.6) nm, very close to the value expected from the design. The results suggest that codeposition of our fiducial provides a convenient and straightforward way to obtain accurate, high-resolution, tip-corrected images.

***In Situ* Image Correction for DNA−Protein Complexes.** To demonstrate the applicability of our method to macromolecular complexes beyond DNA origami, we codeposit our fiducial with double-stranded DNA and a DNA-interacting protein (HIV-1 integrase). We find that the fiducial is biocompatible and preserves its shape despite the presence of DNA-interacting proteins (Figure 5a). Here again,

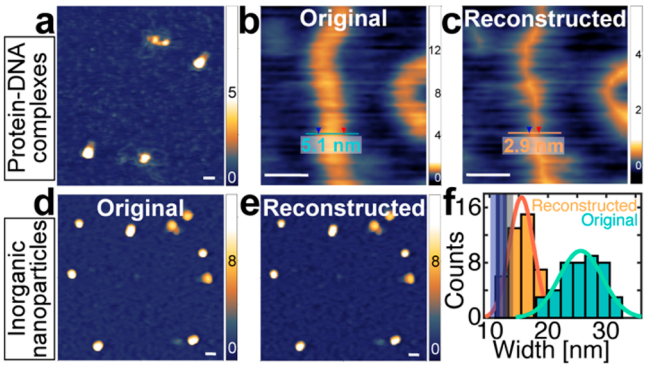

Figure 5. Fiducials enable accurate AFM measurements of DNA protein complexes and inorganic nanoparticles. (a) AFM height image of the fiducial structures codeposited with DNA−protein complexes (DNA length 4.8 kbp; protein HIV−I integrase) deposited on APS mica and measured dry with a resolution of 0.4 pixel/nm. (b) Zoom-in on a different spot of the same sample shown in panel a. The resolution is 1.4 pixel/nm. The apparent DNA width of 5.1 nm is significantly larger than the expected DNA width of 2 nm. (c) The same image as in panel b, after reconstruction based on the tip shape from blind tip reconstruction. The DNA width in the reconstructed AFM image is much closer to the expected DNA width of 2 nm. The scale bars are 10 nm, and *z*-ranges are indicated in nm on the right. (d) AFM height image of the fiducial structures codeposited with SiO_2 nanoparticles, both at a concentration of 1 nM, deposited on APS mica and measured dry with a resolution of 1 pixel/nm. (e) The same image as in panel d, after reconstruction based on the tip shape from blind tip reconstruction using the codeposited fiducials. The scale bars are 50 nm, and *z*-ranges are indicated in nm on the right. (f) Width distribution from AFM images before (turquoise) and after (orange) image reconstruction. The solid lines are Gaussian fits. The width of (25.6 ± 3.7) nm (mean ± std) is corrected to (15.5 ± 2.1) nm by finite tip size correction. This value is much closer to the AFM imaged height (12.6 ± 1.4) nm (mean ± std), indicated with a dark gray vertical line and the standard deviation in light gray, and also to the width measured in TEM, (11.5 ± 1.2) nm, indicated by a dark blue vertical line and the standard deviation in light blue.

we observed that the widths of DNA, protein, and protein−DNA complexes are reduced after image reconstruction. As a proof of principle, we compared the DNA width before and after reconstruction and find that it reduces significantly from ∼5.1 nm to ∼2.9 nm (Figure 5b,c), which is much closer to 2 nm, the crystallographic width of double-stranded DNA.

Height and Width Analysis of Inorganic Nanoparticles. Next, we test our fiducial structure for *in situ* image reconstruction of inorganic nanoparticles. We codeposited SiO_2 nanoparticles with our fiducial. Similar to that for the biological samples, the apparent widths of the silica nanoparticles are significantly larger than the widths in the corrected image (Figure 5d−f). After image reconstruction, the width is reduced from (25.6 ± 3.7) nm (mean ± std) to (15.5 ± 2.1) nm, which is much closer to the width measured in TEM images (11.5 ± 1.2) nm (Supporting Figure S6a,b) and also to the height of the particles measured in AFM, (12.6 ± 1.4) nm (Supporting InformationFigure S6c,d). After image correction, the AFM-determined width and height measurements and the TEM-derived widths are in overall approximate agreement, as would be expected for spherical particles. The fact that the dimensions from the TEM analysis are still slightly smaller than AFM-derived values might be due to the fact that the ultrahigh vacuum used during TEM imaging leads to a small reduction in particle size.[58] The remaining small difference between AFM-determined width and height might stem from imperfections in the image correction, from slight compression of the particle by the AFM cantilever, or could be due to the fact that particles are not perfectly spherical and tend to adhere to the surface with their larger side. Additionally, we observe that the width distribution becomes smaller after image reconstruction (Figure 5f), while the height distribution stays the same within error (Supporting InformationFigure S6d). The reduction in the variance of the width distribution is likely due to an asymmetry of the tip, such that the widths of the particles are distributed wider in the original image than in the reconstructed image.

In conclusion, we have established a method to correct for the finite size of the AFM tip and its specific shape while scanning a sample, employing a DNA origami staircase structure as a fiducial for AFM image calibration. We demonstrate that our fiducial structures are versatile and biocompatible, can be deposited on various surfaces including bare mica, APS mica, and PLL mica, and can be imaged in liquid or dry. This allows straightforward surface codeposition with samples of interest. We demonstrate the broad applicability of the method by imaging DNA origami structures, DNA−protein complexes, and silica nanoparticles. In all cases, the blind tip reconstruction using our fiducial allows for subsequent correction of images for finite tip size, which enables much more accurate determination of sample dimensions than uncorrected images. We show that as few as 10 fiducial structures are sufficient for a good tip estimate. Also, we demonstrate that to characterize the very edge of the tip of FASTSCAN-A cantilevers the fiducial sample gives a better estimate of the effective tip shape than a commercial polycrystalline characterization sample (Supporting Figure S5). In addition, we provide a detailed step-by-step protocol on how to perform the analysis with SPIP or Gwyddion (Methods and Supporting Figure S7). Taken together, our method enables accurate, straightforward, and user-friendly AFM image correction.

We anticipate many new applications coming within reach by using DNA origami structures as fiducials for 3D AFM image calibration. We note that the design of the DNA origami structure could be altered or extended for specific purposes, for example, by addition of additional steps or attachment of fluorescent dyes. A combination with fluorescent markers has the potential to enable simultaneous use of the fiducial for tip shape and fluorescence calibration.[40−43,59,60] Another research direction would be to go beyond imaging and to use the fiducial as a mechanical stiffness marker to study the

https://doi.org/10.1021/acs.nanolett.2c04299
Nano Lett. 2023, 23, 1236−1243

compliance of biomolecules to indentation forces,[61] e.g., to probe the effects of silicification[62,63] or other functionalizations. Soft biological materials are deformed by interactions with the AFM tip, and our fiducial structure could provide a convenient reference to take these effects into account while correcting images. Further, structures on or within the fiducial could be used to quantify and optimize the resolution of AFM images, in addition to concurrently correcting the lateral dimensions. We, therefore, anticipate that our fiducial marker will provide a multimodal calibration platform for a range of applications.

■ ASSOCIATED CONTENT

Supporting Information

The Supporting Information is available free of charge at https://pubs.acs.org/doi/10.1021/acs.nanolett.2c04299.

Materials and Methods, Supporting Table S1, and Supporting Figures S1−S7 (PDF)

Origami design specifications (ZIP)

Example AFM images (ZIP)

■ AUTHOR INFORMATION

Corresponding Authors

Irina V. Martynenko − *Department of Physics and Center for NanoScience, LMU Munich, 80799 Munich, Germany;* orcid.org/0000-0001-5239-3043; Email: irina.martynenko@physik.uni-muenchen.de

Jan Lipfert − *Department of Physics and Center for NanoScience, LMU Munich, 80799 Munich, Germany; Department of Physics and Debye Institute for Nanomaterials Science, Utrecht University, 3584 CC Utrecht, The Netherlands;* orcid.org/0000-0003-3613-7896; Email: j.lipfert@uu.nl

Authors

Pauline J. Kolbeck − *Department of Physics and Center for NanoScience, LMU Munich, 80799 Munich, Germany; Department of Physics and Debye Institute for Nanomaterials Science, Utrecht University, 3584 CC Utrecht, The Netherlands*

Mihir Dass − *Department of Physics and Center for NanoScience, LMU Munich, 80799 Munich, Germany*

Relinde J. A. van Dijk-Moes − *Department of Physics and Debye Institute for Nanomaterials Science, Utrecht University, 3584 CC Utrecht, The Netherlands*

Kelly J. H. Brouwer − *Department of Physics and Debye Institute for Nanomaterials Science, Utrecht University, 3584 CC Utrecht, The Netherlands;* orcid.org/0000-0001-9422-8062

Alfons van Blaaderen − *Department of Physics and Debye Institute for Nanomaterials Science, Utrecht University, 3584 CC Utrecht, The Netherlands*

Willem Vanderlinden − *Department of Physics and Center for NanoScience, LMU Munich, 80799 Munich, Germany; Department of Physics and Debye Institute for Nanomaterials Science, Utrecht University, 3584 CC Utrecht, The Netherlands*

Tim Liedl − *Department of Physics and Center for NanoScience, LMU Munich, 80799 Munich, Germany;* orcid.org/0000-0002-0040-0173

Complete contact information is available at: https://pubs.acs.org/10.1021/acs.nanolett.2c04299

Author Contributions

P.J.K. and W.V. designed this study. M.D. and I.M. designed, assembled, and purified DNA origami samples; R.J.A.v.D-M., K.J.H.B., and A.v.B. synthesized and characterized silica nanoparticles; P.J.K. and W.V. performed AFM measurements and analyzed the data. T.L. and J.L. supervised research; P.J.K. and J.L. wrote the manuscript with input from all authors.

Funding

This work was supported by the Deutsche Forschungsgemeinschaft (DFG, German Research Foundation) through SFB 863, Project 111166240 A11, by Utrecht University, by the Federal Ministry of Education and Research (BMBF) and the Free State of Bavaria under the Excellence Strategy of the Federal Government and the Länder through the ONE MUNICH Project Munich Multiscale Biofabrication, and by the European Union's Horizon 2020 research and innovation program under the Marie Sklodowska-Curie Grant No. 765703.

Notes

The authors declare no competing financial interest.

■ ACKNOWLEDGMENTS

We thank Thomas Nicolaus for laboratory assistance; Diogo Saraiva, Lisa Tran, Steven de Feyter, and Aidin Lak for helpful discussions; and Arthur Ermatov for critical reading of the manuscript.

■ REFERENCES

(1) Binnig, G.; Quate, C. F.; Gerber, C. Atomic Force Microscope. *Phys. Rev. Lett.* **1986**, *56* (9), 930−933.

(2) Hansma, H. G.; Hoh, J. H. Biomolecular Imaging with the Atomic Force Microscope. *Annu. Rev. Biophys. Biomol. Struct.* **1994**, *23* (1), 115−140.

(3) García, R.; Pérez, R. Dynamic atomic force microscopy methods. *Surf. Sci. Rep.* **2002**, *47* (6), 197−301.

(4) Giessibl, F. J. Advances in atomic force microscopy. *Rev. Mod. Phys.* **2003**, *75* (3), 949−983.

(5) Fuentes-Perez, M. E.; Dillingham, M. S.; Moreno-Herrero, F. AFM volumetric methods for the characterization of proteins and nucleic acids. *Methods* **2013**, *60* (2), 113−121.

(6) Ando, T.; Uchihashi, T.; Kodera, N. High-Speed AFM and Applications to Biomolecular Systems. *Annual Review of Biophysics* **2013**, *42* (1), 393−414.

(7) Heath, G. R.; Kots, E.; Robertson, J. L.; Lansky, S.; Khelashvili, G.; Weinstein, H.; Scheuring, S. Localization atomic force microscopy. *Nature* **2021**, *594* (7863), 385−390.

(8) Pyne, A. L. B.; Noy, A.; Main, K. H. S.; Velasco-Berrelleza, V.; Piperakis, M. M.; Mitchenall, L. A.; Cugliandolo, F. M.; Beton, J. G.; Stevenson, C. E. M.; Hoogenboom, B. W.; Bates, A. D.; Maxwell, A.; Harris, S. A. Base-pair resolution analysis of the effect of supercoiling on DNA flexibility and major groove recognition by triplex-forming oligonucleotides. *Nat. Commun.* **2021**, *12* (1), 1053.

(9) Moreno-Herrero, F.; de Jager, M.; Dekker, N. H.; Kanaar, R.; Wyman, C.; Dekker, C. Mesoscale conformational changes in the DNA-repair complex Rad50/Mre11/Nbs1 upon binding DNA. *Nature* **2005**, *437* (7057), 440−443.

(10) Lyubchenko, Y.; Shlyakhtenko, L.; Harrington, R.; Oden, P.; Lindsay, S. Atomic force microscopy of long DNA: imaging in air and under water. *Proc. Natl. Acad. Sci. U. S. A.* **1993**, *90* (6), 2137−2140.

(11) Vanderlinden, W.; Lipfert, J.; Demeulemeester, J.; Debyser, Z.; De Feyter, S. Structure, mechanics, and binding mode heterogeneity of LEDGF/p75−DNA nucleoprotein complexes revealed by scanning force microscopy. *Nanoscale* **2014**, *6* (9), 4611−4619.

(12) Brouns, T.; De Keersmaecker, H.; Konrad, S. F.; Kodera, N.; Ando, T.; Lipfert, J.; De Feyter, S.; Vanderlinden, W. Free Energy

Landscape and Dynamics of Supercoiled DNA by High-Speed Atomic Force Microscopy. *ACS Nano* **2018**, *12* (12), 11907−11916.
(13) Konrad, S. F.; Vanderlinden, W.; Lipfert, J. Quantifying epigenetic modulation of nucleosome breathing by high-throughput AFM imaging. *Biophys. J.* **2022**, *121* (5), 841−851.
(14) Radmacher, M; Tillamnn, R.; Fritz, M; Gaub, H. From Molecules to Cells: Imaging Soft Samples with the Atomic Force Microscope. *Science* **1992**, *257* (5078), 1900−1905.
(15) Konrad, S. F.; Vanderlinden, W.; Frederickx, W.; Brouns, T.; Menze, B. H.; De Feyter, S.; Lipfert, J. High-throughput AFM analysis reveals unwrapping pathways of H3 and CENP-A nucleosomes. *Nanoscale* **2021**, *13* (10), 5435−5447.
(16) Müller, D. J.; Dufrêne, Y. F. Atomic force microscopy as a multifunctional molecular toolbox in nanobiotechnology. *Nat. Nanotechnol.* **2008**, *3* (5), 261−269.
(17) Villarrubia, J. S. Algorithms for Scanned Probe Microscope Image Simulation, Surface Reconstruction, and Tip Estimation. *J. Res. Natl. Inst Stand Technol.* **1997**, *102* (4), 425−454.
(18) Vorselen, D.; Kooreman, E. S.; Wuite, G. J. L.; Roos, W. H. Controlled tip wear on high roughness surfaces yields gradual broadening and rounding of cantilever tips. *Sci. Rep.* **2016**, *6* (1), 36972.
(19) Pyne, A.; Thompson, R.; Leung, C.; Roy, D.; Hoogenboom, B. W. Single-Molecule Reconstruction of Oligonucleotide Secondary Structure by Atomic Force Microscopy. *Small* **2014**, *10* (16), 3257−3261.
(20) Matsunaga, Y.; Fuchigami, S.; Ogane, T.; Takada, S. End-to-End Differentiable Blind Tip Reconstruction for Noisy Atomic Force Microscopy Images. *bioRxiv* **2022**, DOI: 10.1101/2022.09.24.509314.
(21) Danzebrink, H. U.; Koenders, L.; Wilkening, G.; Yacoot, A.; Kunzmann, H. Advances in Scanning Force Microscopy for Dimensional Metrology. *CIRP Annals* **2006**, *55* (2), 841−878.
(22) Xu, M.; Fujita, D.; Onishi, K. Reconstruction of atomic force microscopy image by using nanofabricated tip characterizer toward the actual sample surface topography. *Rev. Sci. Instrum.* **2009**, *80* (4), 043703.
(23) Fuentes-Perez, M. E.; Gwynn, E. J.; Dillingham, M. S.; Moreno-Herrero, F. Using DNA as a fiducial marker to study SMC complex interactions with the atomic force microscope. *Biophysical journal* **2012**, *102* (4), 839−848.
(24) Winzer, A. T.; Kraft, C.; Bhushan, S.; Stepanenko, V.; Tessmer, I. Correcting for AFM tip induced topography convolutions in protein-DNA samples. *Ultramicroscopy* **2012**, *121*, 8−15.
(25) Trinh, M.-H.; Odorico, M.; Bellanger, L.; Jacquemond, M.; Parot, P.; Pellequer, J.-L. Tobacco mosaic virus as an AFM tip calibrator. *Journal of Molecular Recognition* **2011**, *24* (3), 503−510.
(26) Bellotti, R.; Picotto, G. B.; Ribotta, L. AFM Measurements and Tip Characterization of Nanoparticles with Different Shapes. *Nanomanufacturing and Metrology* **2022**, *5* (2), 127−138.
(27) Chen, M.; Parot, J.; Hackley, V. A.; Zou, S.; Johnston, L. J. AFM characterization of cellulose nanocrystal height and width using internal calibration standards. *Cellulose* **2021**, *28* (4), 1933−1946.
(28) Rothemund, P. W. K. Folding DNA to create nanoscale shapes and patterns. *Nature* **2006**, *440* (7082), 297−302.
(29) Seeman, N. C. An overview of structural DNA nanotechnology. *Molecular biotechnology* **2007**, *37* (3), 246.
(30) Douglas, S. M.; Dietz, H.; Liedl, T.; Högberg, B.; Graf, F.; Shih, W. M. Self-assembly of DNA into nanoscale three-dimensional shapes. *Nature* **2009**, *459* (7245), 414−418.
(31) Jungmann, R.; Liedl, T.; Sobey, T. L.; Shih, W.; Simmel, F. C. Isothermal Assembly of DNA Origami Structures Using Denaturing Agents. *J. Am. Chem. Soc.* **2008**, *130* (31), 10062−10063.
(32) Rajendran, A.; Endo, M.; Sugiyama, H. Single-Molecule Analysis Using DNA Origami. *Angew. Chem., Int. Ed.* **2012**, *51* (4), 874−890.
(33) Fisher, P. D. E.; Shen, Q.; Akpinar, B.; Davis, L. K.; Chung, K. K. H.; Baddeley, D.; Šarić, A.; Melia, T. J.; Hoogenboom, B. W.; Lin, C.; Lusk, C. P. A Programmable DNA Origami Platform for Organizing Intrinsically Disordered Nucleoporins within Nanopore Confinement. *ACS Nano* **2018**, *12* (2), 1508−1518.
(34) Andersen, E. S.; Dong, M.; Nielsen, M. M.; Jahn, K.; Lind-Thomsen, A.; Mamdouh, W.; Gothelf, K. V.; Besenbacher, F.; Kjems, J. DNA Origami Design of Dolphin-Shaped Structures with Flexible Tails. *ACS Nano* **2008**, *2* (6), 1213−1218.
(35) Scheckenbach, M.; Schubert, T.; Forthmann, C.; Glembockyte, V.; Tinnefeld, P. Self-Regeneration and Self-Healing in DNA Origami Nanostructures. *Angew. Chem., Int. Ed.* **2021**, *60* (9), 4931−4938.
(36) Thamm, S.; Slesiona, N.; Dathe, A.; Csáki, A.; Fritzsche, W. AFM-Based Probing of the Flexibility and Surface Attachment of Immobilized DNA Origami. *Langmuir* **2018**, *34* (49), 15093−15098.
(37) Kuzuya, A.; Sakai, Y.; Yamazaki, T.; Xu, Y.; Komiyama, M. Nanomechanical DNA origami 'single-molecule beacons' directly imaged by atomic force microscopy. *Nat. Commun.* **2011**, *2* (1), 449.
(38) Niekamp, S.; Stuurman, N.; Vale, R. D. A 6-nm ultra-photostable DNA FluoroCube for fluorescence imaging. *Nat. Methods* **2020**, *17* (4), 437−441.
(39) Blanchard, A. T.; Li, Z.; Duran, E. C.; Scull, C. E.; Hoff, J. D.; Wright, K. R.; Pan, V.; Walter, N. G. Ultra-photostable DNA FluoroCubes: Mechanism of Photostability and Compatibility with FRET and Dark Quenching. *Nano Lett.* **2022**, *22* (15), 6235−6244.
(40) Scheckenbach, M.; Bauer, J.; Zähringer, J.; Selbach, F.; Tinnefeld, P. DNA origami nanorulers and emerging reference structures. *APL Materials* **2020**, *8* (11), 110902.
(41) Raab, M.; Schmied, J. J.; Jusuk, I.; Forthmann, C.; Tinnefeld, P. Fluorescence Microscopy with 6 nm Resolution on DNA Origami. *ChemPhysChem* **2014**, *15* (12), 2431−2435.
(42) Schmied, J. J.; Raab, M.; Forthmann, C.; Pibiri, E.; Wünsch, B.; Dammeyer, T.; Tinnefeld, P. DNA origami−based standards for quantitative fluorescence microscopy. *Nat. Protoc.* **2014**, *9* (6), 1367−1391.
(43) Steinhauer, C.; Jungmann, R.; Sobey, T. L.; Simmel, F. C.; Tinnefeld, P. DNA origami as a nanoscopic ruler for super-resolution microscopy. *Angew. Chem., Int. Ed. Engl.* **2009**, *48* (47), 8870−3.
(44) Engelen, W.; Dietz, H. Advancing Biophysics Using DNA Origami. *Annual Review of Biophysics* **2021**, *50* (1), 469−492.
(45) Shih, W. M.; Lin, C. Knitting complex weaves with DNA origami. *Curr. Opin. Struct. Biol.* **2010**, *20* (3), 276−282.
(46) Ke, Y.; Douglas, S. M.; Liu, M.; Sharma, J.; Cheng, A.; Leung, A.; Liu, Y.; Shih, W. M.; Yan, H. Multilayer DNA Origami Packed on a Square Lattice. *J. Am. Chem. Soc.* **2009**, *131* (43), 15903−15908.
(47) Ray, A.; Liosi, K.; Ramakrishna, S. N.; Spencer, N. D.; Kuzuya, A.; Yamakoshi, Y. Single-Molecule AFM Study of DNA Damage by 1O2 Generated from Photoexcited C60. *J. Phys. Chem. Lett.* **2020**, *11* (18), 7819−7826.
(48) Nickels, P. C.; Wünsch, B.; Holzmeister, P.; Bae, W.; Kneer, L. M.; Grohmann, D.; Tinnefeld, P.; Liedl, T. Molecular force spectroscopy with a DNA origami−based nanoscopic force clamp. *Science* **2016**, *354* (6310), 305−307.
(49) Vanderlinden, W.; Brouns, T.; Walker, P. U.; Kolbeck, P. J.; Milles, L. F.; Ott, W.; Nickels, P. C.; Debyser, Z.; Lipfert, J. The free energy landscape of retroviral integration. *Nat. Commun.* **2019**, *10* (1), 4738.
(50) Zhao, H.; Zhang, Y.; Zhang, S. B.; Jiang, C.; He, Q. Y.; Li, M. Q.; Qian, R. L. The structure of the nucleosome core particle of chromatin in chicken erythrocytes visualized by using atomic force microscopy. *Cell Research* **1999**, *9* (4), 255−260.
(51) Pietkiewicz, J.; Dzierzba, K.; Bronowicka-Szydełko, A.; Staniszewska, M.; Bartyś, A.; Gamian, A. Preparation of bovine serum albumin monomee. for conjugation experiments by using different types of chromatography media. *Journal of Liquid Chromatography & Related Technologies* **2013**, *36* (5), 658−670.
(52) Korpelainen, V.; Linko, V.; Seppä, J.; Lassila, A.; Kostiainen, M. A. DNA origami structures as calibration standards for nano-metrology. *Measurement Science and Technology* **2017**, *28* (3), 034001.
(53) Fischer, S.; Hartl, C.; Frank, K.; Rädler, J. O.; Liedl, T.; Nickel, B. Shape and Interhelical Spacing of DNA Origami Nanostructures

https://doi.org/10.1021/acs.nanolett.2c04299
Nano Lett. 2023, 23, 1236−1243

Studied by Small-Angle X-ray Scattering. *Nano Lett.* **2016**, *16* (7), 4282−4287.
(54) Bruetzel, L. K.; Gerling, T.; Sedlak, S. M.; Walker, P. U.; Zheng, W.; Dietz, H.; Lipfert, J. Conformational Changes and Flexibility of DNA Devices Observed by Small-Angle X-ray Scattering. *Nano Lett.* **2016**, *16* (8), 4871−4879.
(55) Lipfert, J.; Doniach, S.; Das, R.; Herschlag, D. Understanding nucleic acid-ion interactions. *Annu. Rev. Biochem.* **2014**, *83*, 813−41.
(56) Bai, X.-c.; Martin, T. G.; Scheres, S. H. W.; Dietz, H. Cryo-EM structure of a 3D DNA-origami object. *Proc. Natl. Acad. Sci. U. S. A.* **2012**, *109* (49), 20012−20017.
(57) Moreno-Herrero, F.; Colchero, J.; Baró, A. M. DNA height in scanning force microscopy. *Ultramicroscopy* **2003**, *96* (2), 167−174.
(58) Tip−Surface Interaction Forces. In *Amplitude Modulation Atomic Force Microscopy*; Wiley-VCH Verlag GmbH & Co. KGaA: Weinheim, Germany; 2010; pp 25−39.
(59) Schlichthaerle, T.; Strauss, M. T.; Schueder, F.; Woehrstein, J. B.; Jungmann, R. DNA nanotechnology and fluorescence applications. *Curr. Opin. Biotechnol.* **2016**, *39*, 41−47.
(60) Frederickx, W.; Rocha, S.; Fujita, Y.; Kennes, K.; De Keersmaecker, H.; De Feyter, S.; Uji-i, H.; Vanderlinden, W. Orthogonal Probing of Single-Molecule Heterogeneity by Correlative Fluorescence and Force Microscopy. *ACS Nano* **2018**, *12* (1), 168−177.
(61) Müller, D. J.; Dumitru, A. C.; Lo Giudice, C.; Gaub, H. E.; Hinterdorfer, P.; Hummer, G.; De Yoreo, J. J.; Dufrêne, Y. F.; Alsteens, D. Atomic Force Microscopy-Based Force Spectroscopy and Multiparametric Imaging of Biomolecular and Cellular Systems. *Chem. Rev.* **2021**, *121* (19), 11701−11725.
(62) Nguyen, L.; Döblinger, M.; Liedl, T.; Heuer-Jungemann, A. DNA-Origami-Templated Silica Growth by Sol−Gel Chemistry. *Angew. Chem., Int. Ed.* **2019**, *58* (3), 912−916.
(63) Ober, M. F.; Baptist, A.; Wassermann, L.; Heuer-Jungemann, A.; Nickel, B. In situ small-angle X-ray scattering reveals strong condensation of DNA origami during silicification. *Nat. Commun.* **2022**, *13* (1), 5668.
(64) Moreno-Herrero, F.; Gomez-Herrero, J., AFM: Basic Concepts. In *Atomic Force Microscopy in Liquid*; Wiley-VCH Verlag GmbH & Co. KGaA: Weinheim, Germany; 2012; pp 1−34.

https://doi.org/10.1021/acs.nanolett.2c04299
Nano Lett. 2023, 23, 1236−1243